Open Access Full Text Article

ORIGINAL RESEARCH

Apolipoprotein E3-mediated cellular uptake of reconstituted high-density lipoprotein bearing core 3, 10, or 17 nm hydrophobic gold nanoparticles

Skylar T Chuang
Young-Seok Shon
Vasanthy Narayanaswami

Department of Chemistry and Biochemistry, California State University Long Beach, Long Beach, CA, USA

Abstract: We have developed a high-density lipoprotein (HDL)-based platform for transport and delivery of hydrophobic gold nanoparticles (AuNPs). The ability of apolipoprotein E3 (apoE3) to act as a high-affinity ligand for the low-density lipoprotein receptor (LDLr) was exploited to gain entry of HDL with AuNPs into glioblastoma cells. AuNPs of 3, 10, and 17 nm diameter, the latter two synthesized by phase transfer process, were solubilized by integration with phospholipids and apoE3, yielding reconstituted HDL (rHDL) bearing AuNPs. Ultraviolet–visible spectra of rHDL-AuNP indicated the presence of stable particles with surface plasmon band at ~530 nm. Transmission electron microscopy (TEM) of rHDL-AuNP revealed roughly spherical particles with AuNPs embedded in the core. The rHDL-AuNP particles displayed robust binding to the LDLr and were internalized by receptor-mediated endocytosis in glioblastoma cells. Confocal microscopy confirmed cellular uptake of AuNPs in the endosomal–lysosomal compartments, while TEM revealed intracellular aggregated AuNPs. Cell viability assay demonstrated that >85% of cells were viable with rHDL-AuNP treatment of 0.1–100 µg/mL for 24 hours. These findings are significant since they offer an effective means of delivering AuNPs across the cell membrane, which is particularly relevant in tumor cells that overexpress LDLr.

Keywords: apolipoprotein E, gold nanoparticles, lipoproteins, HDL, cancer

Introduction

Among the plethora of emerging nanomaterials, gold nanoparticles (AuNPs) are some of the best characterized ones due to their facile synthesis and their applications in drug delivery, imaging, and photothermal therapy.[1–3] Depending on the intended application, AuNPs can be functionalized with various bioconjugates, namely proteins and peptides,[4] nucleic acids,[5] and other biologically relevant molecules.[6,7] Typically, AuNP bioconjugation involves several strategies[8] such as covalent coupling to the surface ligand using reagents such as 1-ethyl-3-(3-dimethylaminopropyl)carboiimide and N-hydroxysuccinimide with biomolecules[7,9,10] or direct conjugation of biomolecules to the Au surface, often achieved by introducing reactive functional groups such as sulfhydryl groups on the side chains of the peptide and allowing the high-affinity Au-S bonding to take place.[11] In addition, conjugation may also involve an initial chemisorption of thiol ligands onto the Au surface, forming a self-assembled monolayer coating of Au thiolates, followed by self-assembly of biomolecules onto the ligands through electrostatic interactions. In general, the ligands include but are not limited

Correspondence: Vasanthy Narayanaswami
Department of Chemistry and Biochemistry, California State University Long Beach, 1250 Bellflower Boulevard, Long Beach, CA 90840, USA
Tel +1 562 985 4953
Fax +1 562 985 8557
Email vas.narayanaswami@csulb.edu

8495

to alkanethiols, di-*n*-alkyl sulfides, cysteines, xanthates, and mercaptoimidazoles.[12] The current work employs the latter strategy, with noncovalent adsorption of apolipoproteins onto thiolated AuNPs, thereby mimicking circulating lipoprotein morphology. This approach does not involve modification of amino acid side chains that may potentially lead to loss of activity of critical biochemical functions of the apolipoprotein.

Several methods exist for the synthesis of AuNP; one of the most popular is the Turkevich method,[13] which uses citrate as both the reductant and the capping agent. The size can be tuned to within 10–100 nm, and the nanoparticles are monodisperse. However, these AuNPs are water-soluble and cannot be used efficiently for lipoprotein conjugation. Alternatively, the Brust–Schiffrin method[14] produces hydrophobic nanoparticles capped by thiolate ligands. The resulting nanoparticles are stable and monodisperse; however, the diameter of the particles produced is only 1–6 nm. It is generally more difficult to obtain hydrophobic noble metal nanoparticles greater than ~10 nm since no convenient direct synthesis method in organic solvent exists.[15] A conventional way is to perform a phase transfer reaction that changes the nanoparticle surface chemistry from polar to nonpolar. This usually requires a surfactant, an intermediate solvent, or a salt.[16,17] Although there are many types of phase transfer approaches, the options for isolating the transferred nanoparticles are limited.[17] The current study addresses this challenge by demonstrating the preparation of isolatable hydrophobic AuNPs through phase transfer reaction that can be readily incorporated into biological detergents such as lipoproteins.

Lipoproteins solubilize and transport lipids in the bloodstream and are composed of a monolayer of amphipathic biomolecules such as apolipoproteins, phospholipids, and cholesterol that enclose a core of neutral lipids such as cholesteryl esters and triglycerides. They are roughly spherical or discoidal in shape with diameters ranging from 10–20 nm for the high-density lipoproteins (HDLs) to 20–80 nm for the low-density lipoproteins (LDLs) and very low-density lipoproteins.[18] This study focuses on the HDL-sized lipoproteins that bear small, exchangeable, and highly flexible apolipoproteins, which respond with conformational alterations to the dynamic interconversion of particles during normal lipid metabolism. Of particular interest for the current study is apolipoprotein E3 (apoE3), an anti-atherogenic protein that plays a critical role in maintaining plasma cholesterol and triglyceride homeostasis and in mediating cholesterol transport in the central nervous system.[19] It is a highly helical

amphipathic protein, composed of 299 amino acids that are folded into two domains: an N-terminal domain, constituted by residues 1–191 that are involved in high-affinity binding to the LDL receptor (LDLr),[20] and a C-terminal domain, encompassing residues 201–299 that engage in high-affinity lipid binding. We take advantage of these properties to design and reconstitute a nascent HDL particle that offers the ability for receptor recognition and a lipid milieu that can accommodate hydrophobic agents such as thiolate-stabilized AuNPs.

Herein, we report the synthesis, isolation, and characterization of the single-chained alkanethiol-capped 10 and 17 nm AuNPs; in addition, 3 nm AuNPs, synthesized using established protocols, are used for comparison. We utilized the amphipathic nature of phospholipids and apoE3 to coat and surface-modify the lipophilic AuNPs and generated biomimetic nanoparticles. We refer to the phospholipid/apoE3 complexes with AuNP core as reconstituted HDL (rHDL) since they resemble spherical HDL in geometry, size range, and overall chemical organization with a hydrophobic core surrounded by amphipathic molecules. The rHDL bearing 3, 10, or 17 nm AuNPs recapitulate the functional features of "empty" rHDL by retaining the ability to bind cell surface-localized LDLr and facilitating receptor-mediated endocytosis in glioblastoma cells.

Materials and methods

Hydrogen tetrachloroaurate (III) (HAuCl$_4$) trihydrate, trisodium citrate, and Tween 20 were purchased from Acros Organics (Morris Plains, NJ, USA); dodecanethiol and tetradecanethiol were obtained from Sigma-Aldrich (St Louis, MO, USA), 1,2-dimyristoyl-*sn*-glycero-3-phosphocholine (DMPC) from Avanti Polar Lipids (Alabaster, AL, USA), and the detergent compatible™ (DC™) and the bicinchoninic protein assay kits from Bio-Rad Laboratories (Hercules, CA, USA). Human brain A172 glioblastoma cells were obtained from American Type Culture Collection (Manassas, VA, USA); DMEM, fetal bovine serum (FBS), and lipoprotein-deficient serum (LPDS) were from Life Technologies (Grand Island, NY, USA). Milli-Q water (Millipore, Bedford, MA, USA) was used throughout.

Synthesis of 3 nm AuNP

The synthesis of 3 nm AuNPs was carried out as described previously.[23] In short, 0.4 mmol of HAuCl$_4$ was dissolved in 20 mL of water and transferred into 40 mL of toluene using 1.5 mmol of tetraoctylammonium bromide (Sigma-Aldrich) as the surfactant. The Au^{3+} ions were reduced in the presence of 0.2 mmol tetradecanethiol by 4.0 mmol of sodium

borohydride and allowed to stir for 2 hours at 25°C to yield AuNPs. The organic phase was collected, and the solvent was dried under a high vacuum using a Büchi RII Rotavapor® (Büchi, Essen, Germany). The crude AuNP was dispersed in acetonitrile, and the solution was vacuum-filtered; the residue containing AuNP was finally washed 5–6 times with ~50 mL acetonitrile and acetone sequentially to remove residual surfactants and ligands.

Synthesis of 10 and 17 nm AuNPs

Citrate-capped AuNP was first synthesized as described by others[22–24] by boiling 1 mM (for 10 nm AuNP) and 0.3 mM (for 17 nm AuNP) $HAuCl_4$ solution to a reflux and reducing the Au^{3+} ions with 39 mM (for 10 nm AuNP) and 24 mM (for 17 nm AuNP) citrate. To carry out the phase transfer reaction, 250 µL of tetradecanethiol and 500 µL of 50% (v/v) Tween 20 were mixed in 5 mL acetone, and the mixture was subsequently treated with 15 mL of citrate-capped AuNP. The mixture was incubated for 15 minutes at 24°C, followed by the addition of HCl to lower the pH to 1.0. The solution was transferred to a tube containing 15 mL of chloroform, shaken vigorously for ~30 seconds, and then left standing for the transfer to occur. The transferred AuNP was dried by rotary evaporation and washed exhaustively with acetone and ethanol through 6 cycles of sonication and centrifugation. The final purified product was readily soluble in chloroform and dichloromethane with sonication.

Expression, isolation, and purification of apoE3

Recombinant human apoE3 bearing a 6X His-tag was overexpressed in *Escherichia coli* BL21 (DE3) pLysS gold cells, isolated, and purified using a nickel-affinity HiTrap™ chelating column (GE Healthcare, Piscataway, NJ, USA) as described previously.[25] Protein purity was confirmed by sodium dodecyl sulfate–polyacrylamide gel electrophoresis (SDS-PAGE) analysis using a 4%–20% gradient acrylamide gel; protein concentration was determined by the Bio-Rad DC™ assay or by measuring the absorbance at 280 nm using a molar extinction coefficient of 44,460 M^{-1} cm^{-1} for apoE3.

Reconstitution of HDL with AuNP

rHDL bearing AuNP (rHDL-AuNP) was prepared by modifying a previously described method for reconstituting HDL.[26] Briefly, DMPC thin film, recombinant apoE3, and AuNP (w/w/w ratio =5:2:3) were cosonicated in a bath sonicator in the presence of PBS (20 mM sodium phosphate, pH 7.4,

containing 150 mM NaCl) and incubated for 16 hours at 24°C. The mixture was centrifuged at 7,000× *g* for 1 hour, the top 9/10ths was discarded and replenished with PBS, and the process was repeated. After the last wash, the bottom fraction was applied to a slurry of cobalt-conjugated Dynabeads® (Thermo Fisher Scientific, Waltham, MA, USA) to capture His-tag/apoE3-associated AuNP by immobilized metal affinity chromatography. This step removed unbound AuNP, AuNP aggregates, and DMPC vesicles. The rHDL-AuNP was eluted with 0.5 M imidazole, and the eluate was washed twice with PBS using 10,000 molecular weight cutoff filters (Millipore) to remove excess imidazole. The process was repeated in multiple batches, and the samples from the final step were pooled, concentrated, and stored at 4°C.

Spectroscopic characterization of AuNP and rHDL-AuNP
Ultraviolet–visible (UV-Vis) spectroscopy
UV-Vis spectra of the various AuNP and rHDL-AuNP samples were recorded between 300 and 800 nm by using a UV-2450 Shimadzu UV-Vis spectrophotometer (Thermo Fisher Scientific) using quartz cells with a path length of 1 cm.

^{1}H nuclear magnetic resonance (NMR) spectroscopy
^{1}H NMR spectra of the AuNP samples in $CDCl_3$ were recorded using Bruker AC400 FT-NMR (Bruker BioSpin Corporation, Billerica, MA, USA) operating at 400 MHz.

Photon correlation spectroscopy
The zeta potential of rHDL-AuNP preparations was measured by photon correlation spectroscopy using a Zetasizer 3000 HSA (Malvern, Herrenberg, Germany). The dynamic light scattering measurements were carried out in PBS at apoE3 concentrations of 1–2 mg/mL at 25°C.

Nondenaturing PAGE
The rHDL and rHDL-AuNP particles (~50 µg protein) were subjected to nondenaturing PAGE by using 4%–20% acrylamide gradient at 48 V for 23 hours and then 60 V for 1 hour at 4°C followed by staining with 0.5% Amido Black. High-molecular-weight protein standard markers (Amersham High Molecular Weight Calibration Kit; GE Healthcare) were used for comparison and size estimation.

Transmission electron microscopy (TEM)
The size and morphology of AuNP and rHDL-AuNP samples were determined by using TEM. For imaging, the particles were deposited onto a 300-mesh copper grid with a carbon

coating (Ted Pella, Inc., Redding, CA, USA) and dried using filter paper before staining with 2% uranyl acetate. The images were obtained with a JEM1200-EX II electron microscope (JEOL, Tokyo, Japan) at 90.0 keV.

LDLr binding activity

To assess LDLr binding, a coimmunoprecipitation (co-IP) assay was performed as described previously using a construct bearing the LDLr ligand binding domains LA3–6 with a c-Myc epitope (soluble LDR [sLDLr]).[26] In short, 10 μg of rHDL or rHDL-AuNP was incubated with 10 μg of sLDLr in the presence of 2 mM Ca^{2+} for 1 hour at 4°C, followed by co-IP with anti-c-Myc agarose. ApoE3 bound to sLDLr was detected by Western blot analysis using horse radish peroxidase (HRP)-conjugated polyclonal apoE antibody; anti-c-Myc antibody (9E10) was used to confirm the presence of LDLr.

rHDL-AuNP uptake

Human glioblastoma A172 cells were cultured in DMEM supplemented with 10% FBS, 50 units/mL penicillin, and 50 μg/mL streptomycin in a humidified incubator with 5% CO_2 at 37°C. The cells were seeded on a cover glass in a 6-well plate with a density of 1×10^6 cells per well; after 24 hours, they were treated with 10% LPDS and allowed to grow for 20 hours at 37°C. For uptake studies, the cells were incubated with 10 μg/mL of rHDL or rHDL-AuNP for 2.5 hours at 37°C. They were washed with Dulbecco's PBS (DPBS), fixed with 3.7% formaldehyde, and permeabilized with 0.2% Triton X-100 for 5 minutes at 37°C. Cellular uptake of apoE3 was followed by immunofluorescence by staining the cells with mAb1D7- and Alexa555-labeled secondary antibody. They were then stained with 4′,6-diamidino-2-phenylindole dihydrochloride in DPBS for visualizing the nuclei. The cells were visualized by confocal laser scanning microscopy (Olympus IX-81; Olympus Corporation, Tokyo, Japan) and imaged via Olympus Fluoview 1000.

TEM was used to visualize internalized AuNPs; the cells were treated with rHDL-AuNP or AuNPs as such in chloroform (1% v/v) added directly to the medium. Following incubation as described above, the cells were fixed with 3% glutaraldehyde for 30 minutes, washed with Sorenson's phosphate buffer 3 times, and then fixed with 1% osmium tetroxide (Electron Microscopy Sciences, Hatfield, PA, USA) for 30 minutes. The fixed cells were washed and subjected to cold ethanol gradient (30%, 50%, 75%, 95%, and 100%) dehydration, followed by the addition of propylene oxide and curing with araldite resin 502 (Electron Microscopy Sciences) at 60°C for 3 days. The coverslips

embedded in the polymer were sectioned in an ultramicrotome. The samples were adsorbed onto 200-mesh copper grids and stained with saturated uranyl acetate and 0.08% Reynold's quick lead citrate for imaging.

Cell morphology and viability

Glioblastoma cells ($\sim 5 \times 10^3$) were seeded in flat-bottom well plates, incubated for 24 hours at 37°C, and treated with 10% LPDS overnight and with rHDL or rHDL-AuNP. Following treatment, the morphology of the cells was examined by bright-field microscopy (Leica DM IRB inverted phase contrast microscope; Leica Microsystems, Wetzlar, Germany), and the images were recorded using a Retiga-2000R digital camera (Surrey, BC, Canada). Cell viability was assessed by MTT assay (Sigma-Aldrich). The cells were incubated with rHDL-AuNP at concentrations varying from 0.1 to 100 μg/mL in 10% LPDS for 24 hours at 37°C, followed by the addition of MTT dye for 4 hours at 37°C. The media were aspirated, and a solubilizing solution of 20% SDS/50% dimethylformamide at pH 4.7 was added to dissolve the formazan crystals. The absorbance was measured at 570 nm on a Varioskan™ spectrophotometer (Thermo Fisher Scientific). Percentage cell viability was calculated as follows: (absorbance of test runs/absorbance of control) ×100. All results reported are expressed as mean ± standard deviation (n=3) unless otherwise specified. Statistical analysis was carried out by using analysis of variance and Student's *t*-test.

Results
10 and 17 nm AuNP synthesis and characterization

The 10 and 17 nm AuNPs were prepared by phase transfer reaction (Figure 1A–C); the nanoparticles were hydrophobic, chloroform-soluble, and readily obtained within a few hours of transfer reaction. The transfer process was made possible with vigorous shaking or mixing for ~30 seconds; the nanoparticles partitioning into the organic phase could be visualized immediately after shaking. Under these conditions, the transfer of AuNPs was complete, and the yield was high (~95% efficiency), with minimal aggregates found in the aqueous layer or the interface.

Figure 1D and E shows UV-Vis spectra of the 10 and 17 nm AuNPs in citrate- and tetradecanethiol-capped states upon purification. The spectra revealed distinct surface plasmon bands (SPBs) at 520 nm for the citrate-capped samples, which underwent a red shift to 537 nm upon capping with tetradecanethiol when the AuNPs were dissolved in chloroform. The 10 and 17 nm AuNPs were
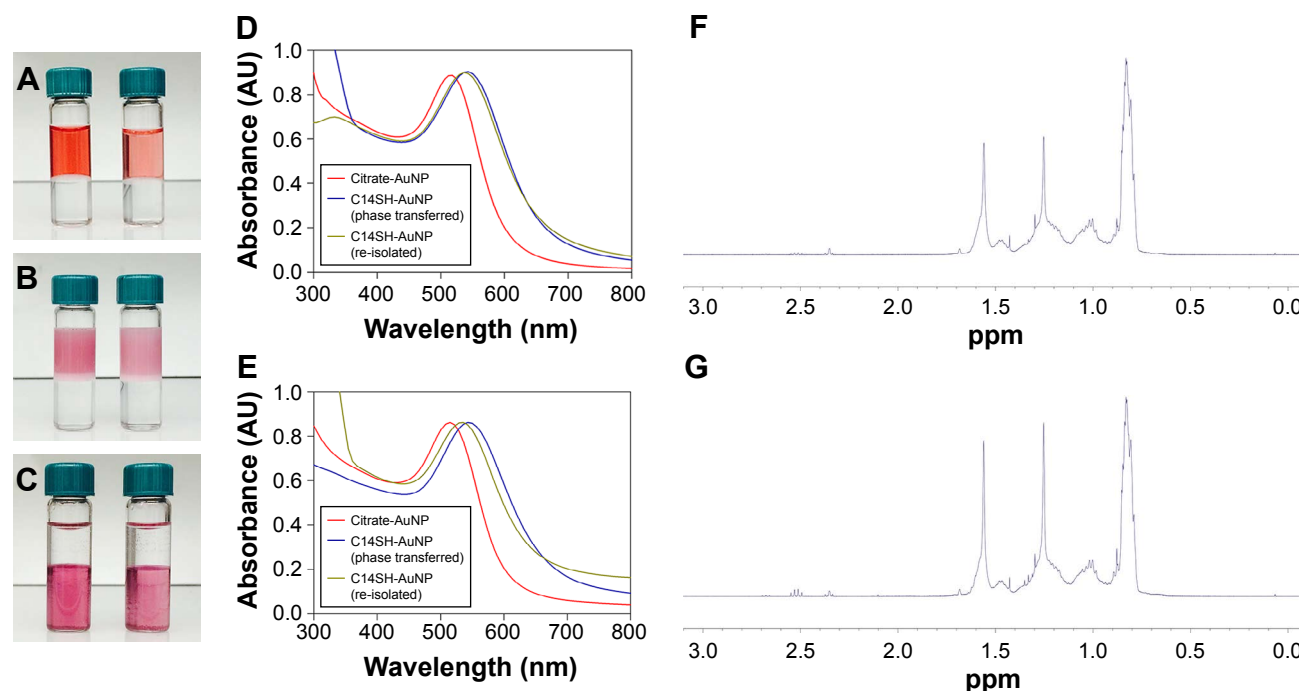
Figure 1 Preparation and spectroscopic characterization of 10 and 17 nm AuNPs. Digital photographs of AuNPs (**A**) prior to transfer, (**B**) activated by acetone/Tween 20/C14SH, (**C**) after transfer. The top and bottom layers represent the aqueous and chloroform layers, respectively. UV-Vis spectra of (**D**) 10 nm and (**E**) 17 nm AuNPs showing the particles in citrate-stabilized state, immediately after phase transfer, and upon reisolation. ^{1}H NMR spectra of purified (**F**) 10 nm and (**G**) 17 nm AuNPs in CDCl$_3$. The signal at 1.6 ppm corresponds to water.
Abbreviations: AuNPs, gold nanoparticles; NMR, nuclear magnetic resonance; UV-Vis, ultraviolet–visible.

stable for at least 1 month when stored at room temperature in a dry form as thin films and could be redissolved in chloroform and dichloromethane after brief sonication. While the AuNPs prepared this way were soluble in other organic solvents such as toluene, tetrahydrofuran, and hexane, their SPBs experienced a red shift in these solvents, especially for hexane, indicating particle aggregation (data not shown). This suggested that alkyl chloride solvents were the most optimal for maintaining particle stability due to their high solvation power and the likely presence of fewer surface-bound citrate species. Furthermore, it was noted that the transfer process occurred efficiently for 30-nm nanoparticles as well, demonstrating the versatility of the transfer method (data not shown). The incomplete citrate exchange during phase transfer of gold colloidal nanoparticles by thiols has been reported by others.[27] Dodecanethiol, a common capping agent, yielded an equally successful transfer (data not shown). Nonetheless, tetradecanethiol was used as the capping agent throughout this study since the chain length matched the fatty acyl chain length of the phospholipid (DMPC) used for reconstituting HDL.

^{1}H NMR spectroscopy was used to confirm adsorption of tetradecanethiol on 10 and 17 nm AuNP (Figure 1F and G, respectively). To obtain a point of comparison for subsequent functional characterization, 3 nm AuNP was synthesized using established protocols.[21] Figures S1 and S2 show the UV-Vis and NMR spectra of tetradecanethiol-capped 3 nm AuNP. For the 10/17 nm AuNPs, the signal at <1 ppm was attributed to the terminal methyl proton on the alkyl chain of tetradecanethiol. The peaks between 1.2 and 1.6 ppm correspond to the methylene protons; the sharp and broad peaks were attributed to the differing environments. Importantly, the absence of a major signal at 2.4 and 2.7 ppm (−CH$_2$S−), which corresponds to free thiols and disulfide, confirmed the near-complete adsorption of tetradecanethiol to the AuNP surface and the absence of free tetradecanethiol in all cases. The minor signal at ~2.4 ppm indicated that a small number of unbound thiols remained at the surface of AuNP despite exhaustive washing.

rHDL-AuNP synthesis and characterization

Figure S3 is a schematic representation of the isolation protocol used to prepare rHDL-AuNP. The 3, 10, and 17 nm AuNPs were cosonicated with DMPC vesicles and apoE3; the His-tag at the N-terminal end of apoE3 was exploited to isolate particles bearing apoE3. DMPC was present in large excess over apoE3 (~150:1, m/m), a ratio at which there was low likelihood of the presence of lipid-free apoE3.

Nevertheless, two centrifugation steps were used to enrich preparations with rHDL-AuNP; they aided in the removal of "empty" DMPC/apoE3 rHDL particles, which have a lower density than AuNP-embedded rHDL and therefore do not readily migrate toward the bottom of the tube. In addition, they served to remove any lipid-free apoE3 by 10-fold "dilution". Subsequently, the samples were treated with cobalt-conjugated Dynabeads separation step that eliminated DMPC vesicles, DMPC vesicles with AuNPs, and free AuNPs (not embedded in rHDL) since they do not have any His-tag/apoE3. Taken together, the combination of centrifugation and Dynabeads capture yielded purified rHDL-AuNP devoid of most of the empty discoidal lipoproteins as well as AuNP aggregates, protein- and AuNP-free lipid vesicles, and free apoE3. Nondenaturing PAGE (Figure S4) revealed relatively more discrete bands for rHDL bearing 10 or 17 nm AuNP compared with rHDL with 3 nm AuNP.

The stability of rHDL-AuNP was evaluated by examining the SPB. rHDL bearing 3, 10, and 17 nm AuNP showed SPB around 520 nm (Figure 2A–C), indicating stable, nonaggregated colloidal Au behavior. The SPBs were particularly evident for rHDL-10- and rHDL-17-nm AuNP, which exhibited sharper and narrower absorption peak, compared with that of the rHDL-3-nm AuNP, which was less pronounced likely due to the smaller size of AuNPs. In the case of rHDL bearing 10 and 17 nm AuNPs, the SPBs were blue-shifted by 15 and 8 nm, respectively, relative to the SPBs of AuNPs alone likely due to the presence of surface lipid and protein conjugation.

Figure 3A–F shows TEM images of AuNP and rHDL-AuNP. The 3, 10, and 17 nm AuNP preparations revealed average diameters of 3.3±1.9, 10.5±1.5, and 17.4±1.4 nm, respectively (Figure 3A–C and G–I). For rHDL-3-nm AuNP (Figure 3D and J), the TEM revealed roughly spheroid structures that were 60–80 nm in diameter with AuNPs of 3.1±0.9 nm embedded inside. rHDL-10- and rHDL-17-nm AuNPs were spherical in shape with a diameter of 22.7±2 and 28.8±2.3 nm, respectively, including the lipoprotein shell (Figure 3E, F, K, and L). The light area around the incorporated AuNPs likely represents the lipoprotein shell. The diameters of the incorporated AuNPs were about the same as free AuNPs (10.2±1.0 and 17.1±1.1 nm, respectively).

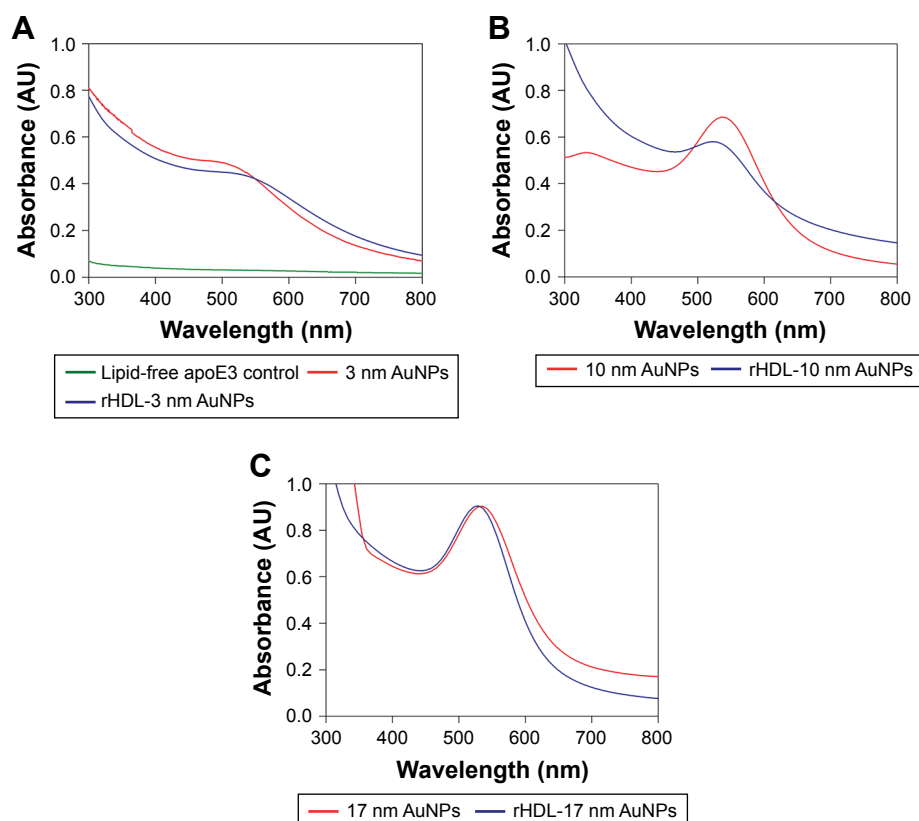The zeta potentials measured for the rHDL and rHDL-3-, rHDL-10-, and rHDL-17-nm AuNP were found

Figure 2 Stability of rHDL-AuNP characterized by SPB. UV-Vis spectra depicting the SPB of rHDL containing (**A**) 3 nm, (**B**) 10 nm, and (**C**) 17 nm AuNPs versus their corresponding core AuNPs. The spectrum of lipid-free apoE3 is shown in panel (**A**).
Abbreviations: AuNPs, gold nanoparticles; rHDL, reconstituted high-density lipoprotein; SPB, surface plasmon band; UV-Vis, ultraviolet–visible.
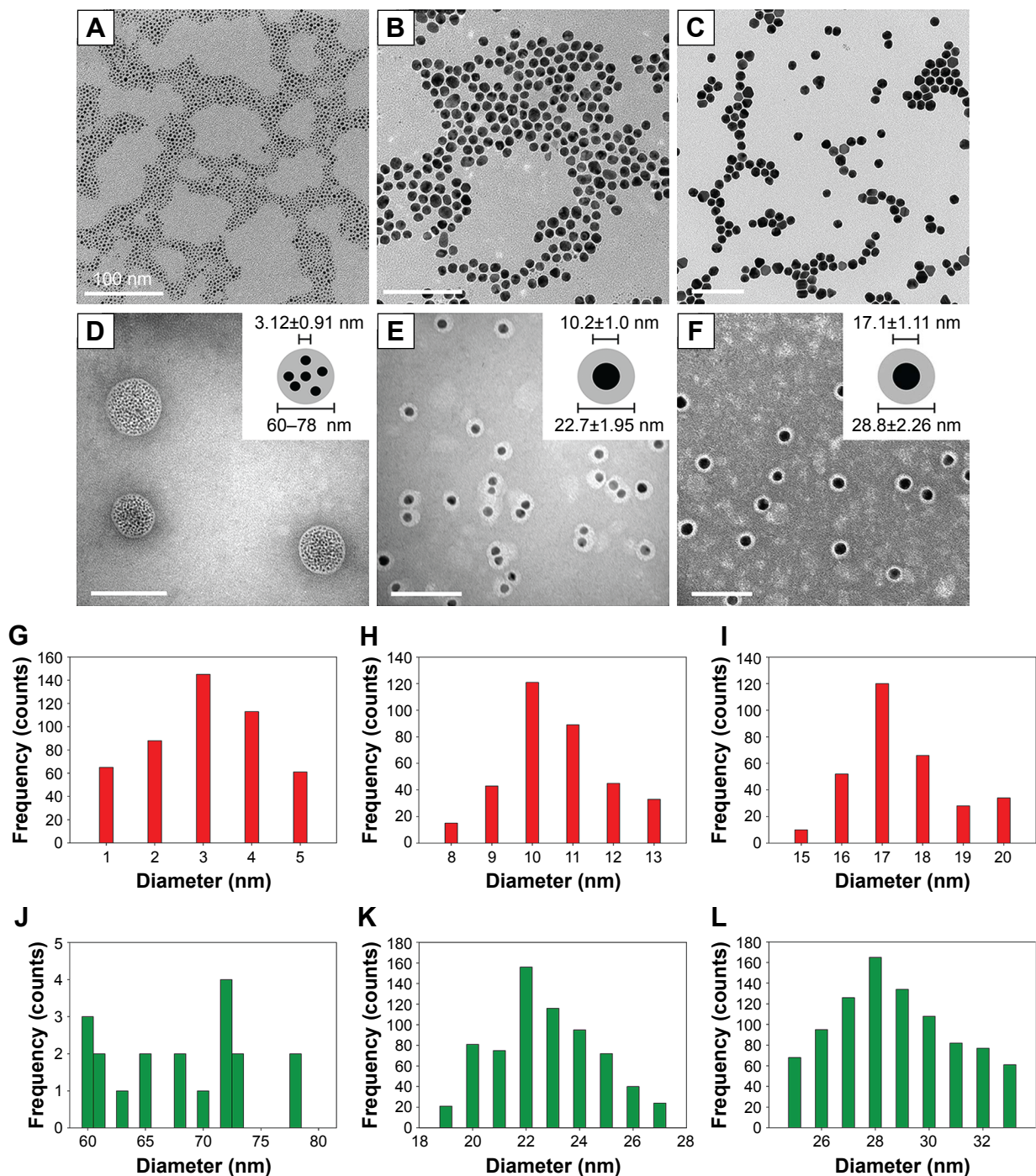
Figure 3 TEM images and histograms of core AuNP and rHDL-AuNP. TEM images of core (**A–C**) and rHDL-AuNP (**D–F**) are shown for 3 nm (**A, D**), 10 nm (**B, E**), and 17 nm (**C, F**) AuNP. The rHDL-AuNP samples were negatively stained with 2% uranyl acetate. All scale bars represent 100 nm. Insets in (Panels **D–F**) show schematic representation of AuNP core and lipoprotein shell that was measured. Histograms depicting size distribution are shown for core (**G–I**) and rHDL-AuNP (**J–L**), with 3 nm (**G, J**), 10 nm (**H, K**), and 17 nm (**I, L**) AuNP.
Abbreviations: AuNPs, gold nanoparticles; rHDL, reconstituted high-density lipoprotein; TEM, transmission electron microscopy.

to be −20.5±1.8, −21.8±0.8, −31.9±6.0, and −22.4±3.4 mV, respectively.

LDLr binding ability of rHDL-AuNP

To assess the LDLr binding ability of rHDL-AuNP, a co-IP assay was performed with c-Myc-sLDLr. The rHDL particles

bearing 3, 10, and 17 nm AuNPs bound to c-Myc-sLDLr were captured by anti-c-Myc antibody-linked agarose beads and detected by anti-apoE3 HRP-conjugated polyclonal antibody or anti-c-Myc antibody (Figure 4, top and bottom, respectively). Receptor-bound apoE3 was noted in the absence or the presence of AuNPs, indicating that the presence of AuNP
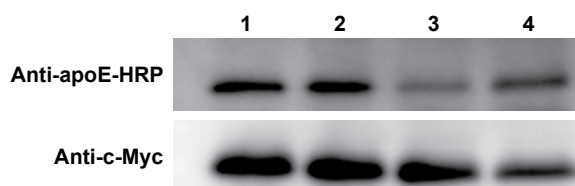
Figure 4 Effects of AuNP on LDLr binding of apoE3. rHDL and rHDL-AuNP (10 μg protein) were incubated with 10 μg of sLDLr at 4°C for 1 hour, followed by co-IP with anti-c-Myc agarose. ApoE3 bound to sLDLr was detected by Western blot using HRP-conjugated polyclonal apoE antibody. The sLDLr was detected by anti-c-Myc antibody for comparison. The lane assignments are as follows: lane 1, rHDL; lane 2, rHDL-3-nm AuNP; lane 3, rHDL-10-nm AuNP; lane 4, rHDL-17-nm AuNP.
Abbreviations: AuNPs, gold nanoparticles; co-IP, coimmunoprecipitation; HRP, horse radish peroxidase; LDLr, low-density lipoprotein receptor; rHDL, reconstituted high-density lipoprotein; sLDLr, soluble LDLr.

does not affect the ability of apoE3 to recognize and bind the sLDLr (Lanes 1–4).

Cellular uptake of rHDL-AuNP

Following confirmation of rHDL-AuNP binding to sLDLr in solution assays, the cellular uptake of the particles was

assessed. The uptake of apoE3 was monitored by immuno-fluorescence while that of AuNP by TEM. Figure 5 shows confocal images of cells incubated with rHDL-3-, rHDL-10-, and rHDL-17-nm AuNPs. Red immunofluorescence (representatives of apoE3) was noted as punctate vesicles in the perinuclear region in all cases, indicative of LDLr-mediated endocytosis. TEM revealed the presence of AuNPs in intracellular sites that appeared to be vesicular structures for all three rHDL-AuNP preparations (Figure 6A–C). In contrast, cells incubated with AuNPs alone did not show any uptake (Figure 6D–F).

Analysis of cell morphology and viability

The cytotoxicity effect of the rHDL-AuNP preparations was assessed by examining the morphology and viability of the glioblastoma cells following treatment with 10 μg/mL rHDL-AuNP for 24 hours at 37°C. Optical microscopy images of the cells following treatment (Figure 7A–D) revealed
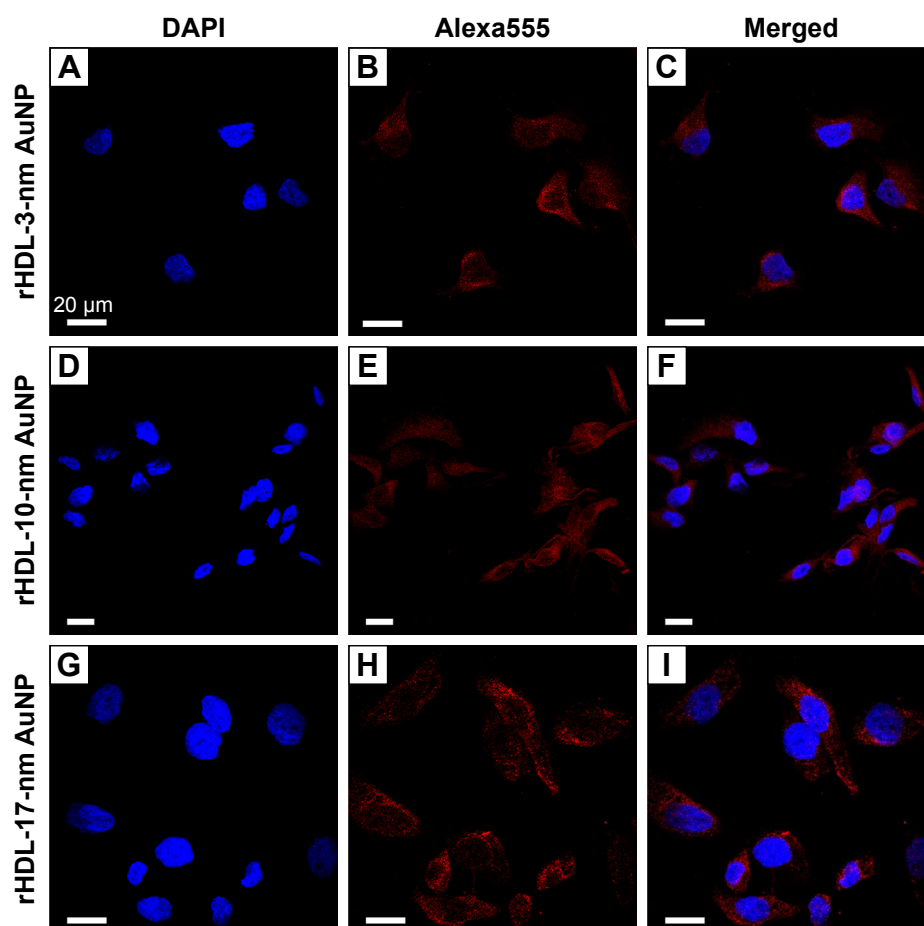

Figure 5 Uptake of rHDL-AuNP by glioblastoma cells. Representative confocal images of glioblastoma cells showing uptake of rHDL-AuNP. Uptake of rHDL-AuNP was visualized by immunofluorescence following the exposure of cells to rHDL-AuNP for 2.5 hours at 37°C: (A–C) rHDL-3-nm AuNP, (D–F) rHDL-10-nm AuNP, and (G–I) rHDL-17-nm AuNP. All scale bars represent 20 μm. The nuclei were visualized by staining with DAPI (panels **A**, **D**, and **G**); apoE3 was visualized using mAb1D7- and Alexa555-labeled secondary antibody (panels **B**, **E**, and **H**); the corresponding merged images are shown in panels (**C**, **F**, and **I**).
Abbreviations: AuNPs, gold nanoparticles; DAPI, 4′,6-diamidino-2-phenylindole dihydrochloride; rHDL, reconstituted high-density lipoprotein.
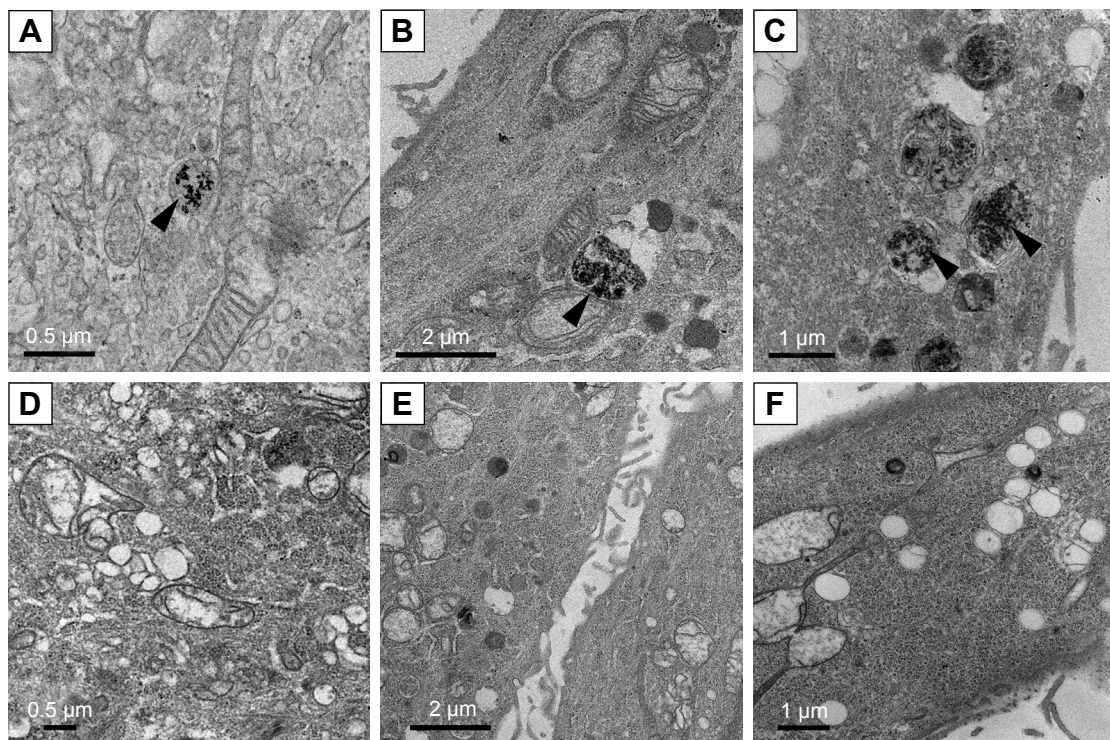
Figure 6 TEM images of cell-internalized rHDL-AuNP and AuNP core. Representative TEM images of thin glioblastoma sections after incubation at 37°C for 2.5 hours with rHDL encompassing (**A**) 3 nm, (**B**) 10 nm, and (**C**) 17 nm AuNPs. Arrowheads draw attention to AuNP aggregates inside endocytic compartments. Control experiments were performed following the same conditions in glioblastoma cells incubated with (**D**) 3 nm, (**E**) 10 nm, and (**F**) 17 nm AuNP core.
Abbreviations: AuNPs, gold nanoparticles; rHDL, reconstituted high-density lipoprotein; TEM, transmission electron microscopy.

no significant changes to the morphology and no signs of blebbing, fragmentation, or shrinkage. The viability of the cells was measured by the MTT assay following the incubation of cells with 0.1–100 μg/mL of rHDL-3-, rHDL-10-, and rHDL-17-nm AuNPs (Figure 7E), where medium was used as the negative control and 1% Triton X-100 as the positive control. The cells were 85%–90% viable at low doses of rHDL-AuNP (0.1–10 μg/mL) used in the current study,
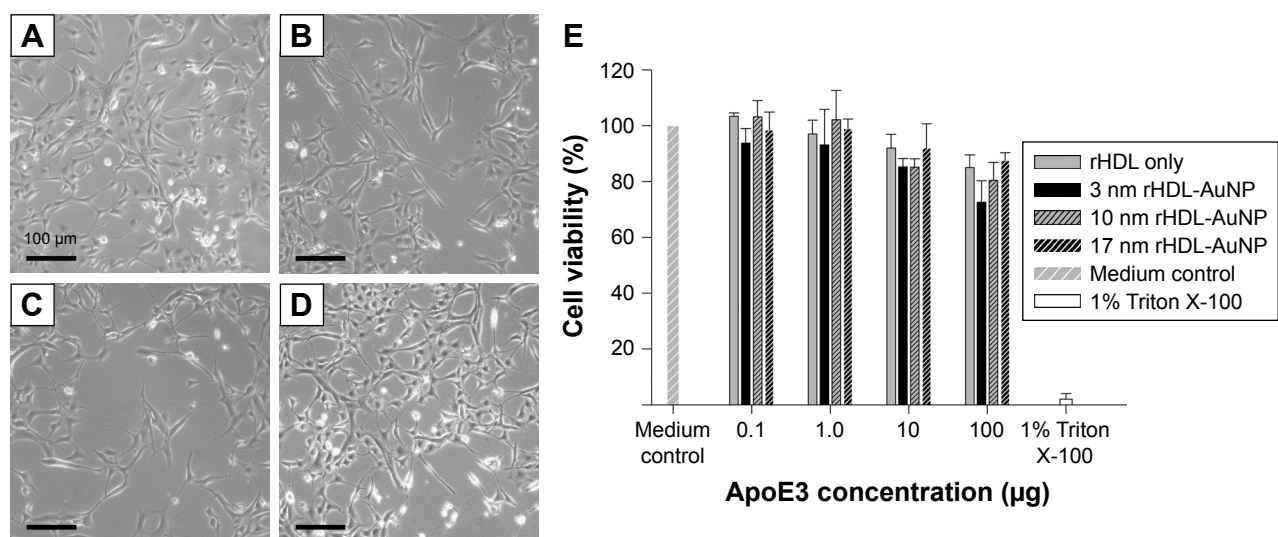
Figure 7 Cell morphology and viability of glioblastoma A172 cells incubated with rHDL-AuNP. Bright field light micrographs of glioblastoma cells with (**A**) no addition and following 24-hour incubation with rHDL containing (**B**) 3 nm, (**C**) 10 nm, and (**D**) 17 nm AuNPs at 37°C. No apparent change in morphology was observed. All scale bars represent 100 μm. (**E**) Cell viability of glioblastoma cells treated with various doses of rHDL-AuNP evaluated using MTT assay following incubation for 24 hours. Values represent mean ± standard deviation (n=3).
Abbreviations: AuNPs, gold nanoparticles; rHDL, reconstituted high-density lipoprotein.

which represent physiologically relevant concentrations of apoE3. There were no significant differences in cell viability between the untreated and 0.1–10 µg/mL treatment for all rHDL-AuNP. At any given dose studied, the viability of cells treated with rHDL-AuNP was similar to those treated with rHDL, regardless of AuNP diameter. At higher dosage (100 µg/mL), there was a significant decrease in viability for rHDL-3-nm AuNPs (P=0.014) when compared to 0.1 µg/mL treatment. Other studies have reported higher cytotoxicity for smaller sized AuNPs (<5 nm).[28]

Discussion

Previous studies demonstrated successful phase transfer and isolation of >10 nm AuNPs;[17] however, a special capping agent, ((Z)-octadec-9-en-1-yl-5-(1,2-dithiolan-3-yl)-pentanoate) was required. They used cetyltrimethylammonium bromide as the surfactant, which is unsuitable for biological applications due to the toxicity of unbound surfactant.[29] In the current study, tetradecanethiol, an alkanethiol ligand, was selected as the capping ligand with the rationale that the long chain length would readily stabilize the particles in nonpolar solvents such as chloroform due to steric repulsion. Alkanethiol ligands are commonly used capping agents in small metal nanoparticle synthesis.[30–32] Tween 20 (Polysorbate 20) was the surfactant of choice due to its wide availability and biocompatibility. Initial attempts were also made by placing tetradecanethiol in the organic layer and Tween 20 with the AuNPs in the aqueous layer; while some transfer was observed, the process was not complete and extensive aggregation was noted at the interface under a wide range of conditions attempted (data not shown).

It was found that mixing tetradecanethiol and Tween 20 first in acetone followed by incubation with AuNPs yielded the most successful transfer. This is likely due to acetone being miscible with water, thereby maximizing contact between AuNPs and the surfactant/capping reagent. Although other reports showed successful transfer using ethanol as the intermediate solvent,[33] we noted AuNP aggregation with this solvent under the conditions used in our studies. Acetone, on the other hand, did not cause AuNP aggregation, allowed favorable mixing and ensured successful transfer into chloroform under acidic pH. However, it was critical to maintain the amount of acetone used at no more than 10 times the volume of Tween 20, to prevent AuNP aggregation during the mixing process. Both 10 and 17 nm AuNPs showed excellent stability after transfer. UV-Vis spectroscopy indicated a SPB at 537 nm, rather than the 520 nm peak commonly observed for stable aqueous colloidal Au. The red shift is attributed to the higher refractive index of chloroform (1.446) compared with that of water (1.333).[34] The AuNP were isolatable, were readily soluble in organic solvents such as chloroform and dichloromethane with brief sonication, and could be stored for weeks in a dry form as thin films.

In ^{1}H NMR spectroscopy, the peak pattern from 0.7 to 1.6 ppm was significantly different (broadened and more abundant signals) between 10/17 and 3 nm AuNPs; this was attributed to the different local proton environments caused by the lower curvature of the larger sized AuNPs. The absence of major signals at 2.4 and 2.7 ppm in all cases was an indication of adsorption of free tetradecanethiol onto the AuNP surface.

The hydrophobic AuNP core appeared to serve as a template in constructing a biomimetic lipoprotein nanoparticle, the rHDL-AuNP. Derivatives of lipoproteins have received widespread attention as delivery systems for therapeutics since they mimic endogenous lipid carriers.[35–37] They are expected to potentially prolong the circulation time of the nanoparticles, leading to greater bioavailability.[35,37] Stability and size are essential considerations for a robust drug delivery system. The rHDL-AuNPs generated in this study satisfied both features; they elicited characteristic SPB peak absorptions near 520 nm, indicative of stable, nonaggregated AuNPs. The SPB for rHDL-3 nm AuNP was less pronounced than those of 10 or 17 nm due to the nature of the smaller sized AuNPs. In the case of the 10 and 17 nm particles, the SPBs were blue-shifted by 15 and 8 nm relative to the SPBs of AuNP alone. The stability of the embedded AuNP was attributed to the phospholipids and proteins that shielded them from the aqueous environment, preventing aggregation. The sizes of the rHDL-AuNP largely depended on the sizes of the hydrophobic AuNP core. With rHDL-3-nm AuNPs, up to 200 AuNPs were enclosed in the core. With rHDL-10-nm AuNP and rHDL-17-nm AuNP, the DMPC likely forms a monolayer around a single AuNP core. This was inferred from TEM data, where the lipoprotein shells, which appeared white due to negative staining, were found as rings around the AuNPs. In all cases, the overall geometric organization was similar to that of a mature spherical HDL, with the cholesteryl ester core of the latter replaced by a single or multiple AuNPs. Similar observations were reported in other studies using 6 and 8 nm AuNPs as the core and apoA1 as the apolipoprotein.[11]

The exact number of apoE3 molecules per rHDL-AuNP or the conformation of the protein in the rHDL-AuNP-bound state is not known; however, it is possible to estimate the number of apoE3 molecules per rHDL-AuNP from the

particle diameter information obtained from TEM. Previous studies from our group examined the ratio of apoE3 to discoidal rHDL with a diameter of ~15 nm.[38] We calculated that 4–6 apoE3 molecules likely circumscribe the rHDL. In the current study, the incorporation of AuNPs appeared to change the particle geometry from discoidal to spherical, a process that was accompanied by an increase in surface area. We estimated that a single rHDL-10- and rHDL-17-nm AuNPs may accommodate ~18 and ~30 molecules of apoE3, respectively. The rHDL-3-nm AuNPs appeared to accommodate ~180 molecules of apoE3 based on the particle size and diameter. Figure 8 shows models of rHDL-AuNP with multiple AuNPs for the smaller 3 nm particles and a single AuNP for the larger 10 and 17 nm AuNPs, with the amphipathic lipids and helices of apoE3 encircling the hydrophobic core.

In addition to stability and size, the particles were further characterized based on their zeta potential. A negative zeta potential is important, as a net cationic charge can enhance cytotoxicity and present destructive effect by interacting with the negative charge of cell membranes.[39–41] The high surface negative charge of the rHDL particles was attributed to the chargeable groups on apoE3 and further ensured colloidal stability.[42] Not surprisingly, drug carriers having a negative charge have been shown to be less toxic[43] and have elicited greater bioavailability.[44]

Many tumors overexpress the LDLr on the cell surface due to increased demand for cholesterol during membrane biogenesis faced by the rapidly proliferating cells.[45–47] The LDLr serves to capture extracellular sources of cholesterol via lipoproteins. In several cases, cancer patients suffer from various degrees of hypocholesterolemia, suggesting a strong inverse correlation between circulating plasma LDL level and the progression of the malignancy. This has been attributed to the increased clearance of LDL by the enhanced LDLr expression.[47] We exploited this property of the tumors to gain entry into the cell via the LDLr for rHDL-AuNP delivery. The higher affinity of apoE3 for LDLr binding (compared with apoB100) was an additional feature that drove the design of the lipoprotein-like "nanovehicle".

The sLDLr binding data indicated that the method of embedding AuNP in rHDL maintained and preserved two key structural and conformational features that are critical for LDLr binding function of apoE3:

1. The LDLr binding sites were unaltered: LDLr binding sites are located in the N-terminal (NT) domain of apoE3, with a cluster of conserved Lys and Arg residues playing a critical role in mediating interaction between apoE3 and the receptor.[48,49] Previous studies have shown that chemical modification or single amino acid substitution resulted in ablation of LDLr binding activity underscoring the importance of these positively charged residues in receptor interaction.[49,50] This feature precluded us from using Traut's reagent (2-iminothiolane), which is a common approach of conjugating lysines onto metallic nanoparticles via sulfhydryl groups.[11,51] The current method of embedding AuNPs during the cosonication with DMPC and apoE3 appeared to have left the basic residues unaffected.

2. The active conformation required for LDLr binding was maintained: An important aspect of LDLr binding of apoE3 is the requirement that it is associated with lipids or lipoproteins, which triggers a conformational change in its NT domain. This domain bears a 4-helix bundle that is
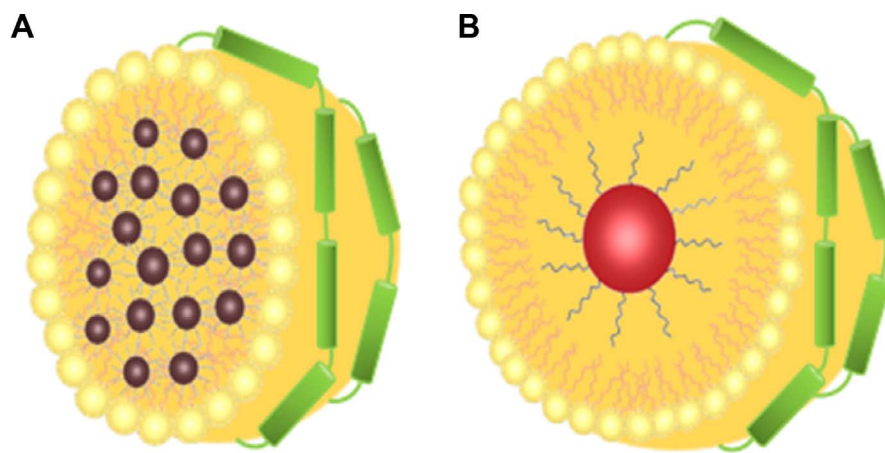

Figure 8 Schematic representation of (**A**) rHDL-3-nm AuNP and (**B**) rHDL-10- or rHDL-17-nm AuNPs.
Abbreviations: AuNPs, gold nanoparticles; rHDL, reconstituted high-density lipoprotein.

composed of 4 long amphipathic α-helices, the nonpolar faces of which are oriented toward the protein interior.[52] Upon lipid interaction, the helix bundle undergoes an opening that allows the nonpolar side to interact with the lipid surface; this step also allows the NT domain to adopt a curvature that is critical for interaction with the LDLr.[53] The current protocol of embedding AuNPs in a lipid environment allowed apoE3 to adopt a conformation that recapitulated the overall lipid-bound conformation with retention of LDLr recognition and binding ability. Cellular uptake studies suggest entry of rHDL-AuNP via the LDLr, as noted in a previous study, wherein we demonstrated binding and cellular uptake of apoE3-containing rHDL loaded with flavonoids via the LDLr in glioblastoma cells based on inhibition by suramin and excess LDL.[26]

Following binding and uptake of rHDL-AuNP in glioblastoma cells, apoE3 appeared as punctate vesicles, in the perinuclear region and in late endosomal and lysosomal vesicles; this suggested that the presence of AuNP did not alter the ability of apoE3 to bind cell surface-localized LDLr (and/or other LDLr family members) and mediate cellular internalization of rHDL with embedded particles. TEM revealed the presence of AuNPs in vesicles, presumably late endosomes and lysosomes, in cells incubated with rHDL-AuNP, but not in those incubated with AuNPs alone under identical conditions. Taken together, it appears that lipid-associated apoE3 facilitated transport of AuNP into the glioblastoma cells to intracellular sites. Interestingly, the internalized rHDL-AuNPs were in an aggregated state (data not shown), possibly due to the unique microenvironment in these organelles. The low pH and the action of proteases, lipases, and esterases in the lysosomes likely hydrolyzed the phospholipids and proteins on the nanoparticle surface. Their combined action would likely expose the hydrophobic AuNP core, leading to particle aggregation in the aqueous environment. This naturally occurring aggregation phenomenon is an appealing feature since aggregated AuNPs present a possible option of applying a photothermal therapeutic strategy. Other researchers demonstrated that formulations of AuNPs functionalized with Erbitux (an anti-epidermal growth factor receptor antibody) lead to targeted endosome and lysosome delivery.[54] The present study relies on apoE3-mediated lipoprotein uptake mechanism adopted by cells to process the rHDL-AuNP.

Conclusion

We report the synthesis of 10 and 17 nm AuNPs by phase transfer process and incorporation of 3, 10, and 17 nm AuNPs into rHDL bearing phospholipids and apoE3 by cosonication method. The presence of apoE3 facilitated binding and entry of AuNPs embedded in rHDL into cells likely via the LDLr family of proteins by virtue of its ability to serve as a high-affinity ligand. The rHDL-AuNP complexes generated by this method were stable and demonstrated transport and delivery potential. Further studies are needed with consideration of the photothermal ability of AuNP aggregates, the potential of combination with finely tuned homing strategies, and chemotherapeutics incorporated into the rHDL-AuNP for the more targeted and efficient destruction of tumor cells.

Disclosure

The authors report no conflicts of interest in this work.

References

1. Sajja HK, East MP, Mao H, Wang AY, Nie S, Yang L. Development of multifunctional nanoparticles for targeted drug delivery and non-invasive imaging of therapeutic effect. *Curr Drug Discov Technol*. 2009;6(1):43–51.
2. Allijn IE, Leong W, Tang J, et al. Gold nanocrystal labeling allows low-density lipoprotein imaging from the subcellular to macroscopic level. *ACS Nano*. 2013;7(11):9761–9770.
3. Madsen SJ, Christie C, Hong SJ, et al. Nanoparticle-loaded macrophage-mediated photothermal therapy: potential for glioma treatment. *Laser Med Sci*. 2015;30(4):1357–1365.
4. Chen G, Xie Y, Peltier R, et al. Peptide-decorated gold nanoparticles as functional nano-capping agent of mesoporous silica container for targeting drug delivery. *ACS Appl Mater Interfaces*. 2016;8(18):11204–11209.
5. Ding Y, Jiang Z, Saha K, et al. Gold nanoparticles for nucleic acid delivery. *Mol Ther*. 2014;22(6):1075–1083.
6. Roux S, Garcia B, Bridot JL, et al. Synthesis, characterization of dihydrolipoic acid capped gold nanoparticles, and functionalization by the electroluminescent luminol. *Langmuir*. 2005;21(6):2526–2536.
7. Zhang Z, Jia J, Lai Y, Ma Y, Weng J, Sun L. Conjugating folic acid to gold nanoparticles through glutathione for targeting and detecting cancer cells. *Bioorg Med Chem*. 2010;18(15):5528–5534.

8. Sapsford KE, Algar WR, Berti L, et al. Functionalizing nanoparticles with biological molecules: developing chemistries that facilitate nanotechnology. *Chem Rev*. 2013;113(3):1904–2074.

9. Oh E, Hong MY, Lee D, Nam SH, Yoon HC, Kim HS. Inhibition assay of biomolecule based on fluorescence resonance energy transfer (FRET) between quantum dots and gold nanoparticles. *J Am Chem Soc*. 2005;127(10):3270–3271.

10. Park JH, Park J, Dembereldorj U, et al. Raman detection of localized transferrin-coated gold nanoparticles inside a single cell. *Anal Bioanal Chem*. 2011;401(5):1631–1639.

11. Luthi AJ, Zhang H, Kim D, Giljohann DA, Mirkin CA, Thaxton CS. Tailoring of biomimetic high-density lipoprotein nanostructures changes cholesterol binding and efflux. *ACS Nano*. 2012;6(1):276–285.

12. Ulman A. Formation and structure of self-assembled monolayers. *Chem Rev*. 1996;96(4):1533–1554.

13. Turkevich J, Stevenson PC, Hillier JA. Study of the nucleation and growth processes in the synthesis of colloidal gold. *J Discuss Faraday Soc*. 1951;11:55–75.

14. Brust M, Walker M, Bethell D, Schiffrin DJ, Whyman R. Synthesis of thiol-derivatised gold nanoparticles in a two-phased liquid-liquid system. *J Chem Soc Chem Commun*. 1994;7:801–802.

15. Goulet PJG, Bourret GR, Lennox RB. Facile phase transfer of large, water-soluble metal nanoparticles to nonpolar solvents. *Langmuir*. 2012; 28(5):2909–2913.

16. Hirai H, Aizawa H. Preparation of stable dispersions of colloidal gold in hexanes by phase transfer. *J Colloid Interface Sci*. 1993;161: 471–474.

17. Lista M, Liu DZ, Mulvaney P. Phase transfer of noble metal nanoparticles to organic solvents. *Langmuir*. 2014;30(8):1932–1938.

18. Getz GS, Reardon CA. Apoprotein E as a lipid transport and signaling protein in the blood, liver, and artery wall. *J Lipid Res*. 2009; 50(Suppl):S156–S161.

19. Vitali C, Wellington CL, Calabresi L. HDL and cholesterol handling in the brain. *Cardiovasc Res*. 2014;103(3):405–413.

20. Wilson C, Wardell MR, Weisgraber KH, Mahley RW, Agard DA. Three dimensional structure of the LDL receptor-binding domain of human apolipoprotein E. *Science*. 1991;252(5014):1817–1822.

21. Isaacs SR, Choo H, Ko WB, Shon YS. Chemical, thermal, and ultrasonic stability of hybrid nanoparticles and nanoparticle multilayer films. *Chem Mater*. 2006;18(1):107–114.

22. Grabar KC, Freeman RG, Hommer MB, Natan MJ. Preparation and characterization of Au colloid monolayers. *Anal Chem*. 1995;67(4): 735–743.

23. Kimling J, Maier M, Okenve B, Kotaidis V, Ballot H, Plech A. Turkevich method for gold nanoparticle synthesis revisited. *J Phys Chem B*. 2006;110(32):15700–15707.

24. Lim II, Mott D, Ip W, et al. Interparticle interactions in glutathione mediated assembly of gold nanoparticles. *Langmuir*. 2008;24(16): 8857–8863.

25. Bains GK, Kim SH, Sorin EJ, Narayanaswami V. Extent of pyrene excimer fluorescence emission is a reflector of distance and flexibility: analysis of the segment linking the LDL receptor-binding and tetramerization domains of apolipoprotein E3. *Biochemistry*. 2012; 51(31):6207–6219.

26. Kim SH, Adhikari BB, Cruz S, Schramm MP, Vinson JA, Narayanaswami V. Targeted intracellular delivery of resveratrol to glioblastoma cells using apolipoprotein E-containing reconstituted HDL as a nanovehicle. *PLoS One*. 2015;10(8):e0135130.

27. Park JW, Shumaker-Parry JS. Structural study of citrate layers on gold nanoparticles: role of intermolecular interactions in stabilizing nanoparticles. *J Am Chem Soc*. 2014;136(5):1907–1921.

28. Pan Y, Neuss S, Leifert A, et al. Size-dependent cytotoxicity of gold nanoparticles. *Small*. 2007;3(11):1941–1949.

29. Wang L, Jiang X, Ji Y, et al. Surface chemistry of gold nanorods: origin of cell membrane damage and cytotoxicity. *Nanoscale*. 2013; 5(18):8384–8391.

30. England CG, Priest T, Zhang G, et al. Enhanced penetration into 3D cell culture using two and three layered gold nanoparticles. *Int J Nanomedicine*. 2013;8:3603–3617.

31. Serrano-Montes AB, Jimenez de Aberasturi D, Langer J, et al. A general method for solvent exchange of plasmonic nanoparticles and self-assembly into SERS-active monolayers. *Langmuir*. 2015; 31(33):9205–9213.

32. Rasch MR, Yu Y, Bosoy C, Goodfellow BW, Korgel BA. Chloroform-enhanced incorporation of hydrophobic gold nanocrystals into dioleoylphosphatidylcholine (DOPC) vesicle membranes. *Langmuir*. 2012; 28(36):12971–12981.

33. Wang X, Xu S, Zhou J, Xu W. A rapid phase transfer method for nanoparticles using alkylamine stabilizers. *J Colloid Interface Sci*. 2010; 348(1):24–28.

34. Pastoriza-Santos I, Hamanaka Y, Fukuta K, Nakamura A, Liz-Marzán LM. Anisotropic silver nanoparticles: synthesis and optical properties. In Liz-Marzán LM, Giersig M, editors. *Low-Dimensional Systems: Theory, Preparation, and Some Applications*. The Netherlands: Kluwer Academic Publishers; 2003:65–75.

35. Ng KK, Lovell JF, Zheng G. Lipoprotein-inspired nanoparticles for cancer theranostics. *Acc Chem Res*. 2011;44(10):1105–1113.

36. Marrache S, Dhar S. Biodegradable synthetic high-density lipoprotein nanoparticles for atherosclerosis. *Proc Natl Acad Sci U S A*. 2013; 110(23):9445–9450.

37. Lacko AG, Nair M, Paranjape S, Johnson S, McConathy WJ. High density lipoprotein complexes as delivery vehicles for anticancer drugs. *Anticancer Res*. 2002;22(4):2045–2049.

38. Fisher CA, Narayanaswami V, Ryan RO. The lipid-associated conformation of the low density lipoprotein receptor binding domain of human apolipoprotein E. *J Biol Chem*. 2000;275(43):33601–33606.

39. Wagner S, Zensi A, Wien SL, et al. Uptake mechanism of ApoE-modified nanoparticles on brain capillary endothelial cells as a blood-brain barrier model. *PLoS One*. 2012;7(3):e32568.

40. Müller RH, Jacobs C, Kayser O. Nanosuspensions as particulate drug formulations in therapy rationale for development and what we can expect for the future. *Adv Drug Deliver Rev*. 2001;47(1): 3–19.

41. Feng SS, Ruanb G, Li QT. Fabrication and characterizations of a novel drug delivery device liposomes-in-microsphere (LIM). *Biomaterials*. 2004;25(21):5181–5189.

42. Qi L, Xu Z, Jiang X, Li Y, Wang M. Cytotoxic activities of chitosan nanoparticles and copper-loaded nanoparticles. *Bioorgan Med Chem Lett*. 2005;15(5):1397–1399.

43. Honary S, Zahir F. Effect of zeta potential on the properties of nano-drug delivery systems – a review (Part 2). *Trop J Pharm Res*. 2013; 12(2):265–273.

44. Unger F, Wittmar M, Kissel T. Branched polyesters based on poly[vinyl-3-(dialkylamino)alkylcarbamate-co-vinyl acetate-covinyl alcohol]-graft-poly(d,l-lactide-co-glycolide): effects of polymer structure on cytotoxicity. *Biomaterials*. 2007;28(9):1610–1619.

45. Nikanjam M, Blakely EA, Bjornstad KA, Shu X, Budinger TF, Forte TM. Synthetic nano-low density lipoprotein as targeted drug delivery vehicle for glioblastoma multiforme. *Int J Pharm*. 2007;328(1): 86–94.

46. Firestone RA. Low-density lipoprotein as a vehicle for targeting antitumor compounds to cancer cells. *Bioconjug Chem*. 1994;5(2): 105–113.

47. Peterson C, Vitols S, Rudling M, Blomgren H, Edsmyr F, Skoog L. Hypocholesterolemia in cancer patients may be caused by elevated LDL receptor activities in malignant cells. *Med Oncol Tumor Pharmacother*. 1985;2(3):143–147.

48. Weisgraber KH. Apolipoprotein E: structure-function relationships. *Adv Protein Chem*. 1994;45:249–302.

49. Zaiou M, Arnold KS, Newhouse YM, et al. Apolipoprotein E-low density lipoprotein receptor interaction: influences of basic residues and amphipathic alpha-helix organization in the ligand. *J Lipid Res*. 2000;41(7):1087–1095.

50. Tran TN, Kosaraju MG, Tamamizu-Kato S, et al. Acrolein modification impairs key functional features of rat apolipoprotein E: identification of modified sites by mass spectrometry. *Biochemistry*. 2014; 53(2):361–375.

51. Kommareddy S, Amiji M. Preparation and evaluation of thiol-modified gelatin nanoparticles for intracellular DNA delivery in response to glutathione. *Bioconjug Chem*. 2005;16(6):1423–1432.

52. Segrest JP, Jones MK, De Loof H, Brouillette CG, Venkatachalapathi YV, Anantharamaiah GM. The amphipathic helix in the exchangeable apolipoproteins: a review of secondary structure and function. *J Lipid Res*. 1992;33(2):141–166.

53. Lu B, Morrow JA, Weisgraber KH. Conformational reorganization of the four-helix bundle of human apolipoprotein E in binding to phospholipid. *J Biol Chem*. 2000;275(27):20775–20781.

54. Hainfeld JF, O'Connor MJ, Lin P, Qian L, Slatkin DN, Smilowitz HM. Infrared-transparent gold nanoparticles converted by tumors to infrared absorbers cure tumors in mice by photothermal therapy. *PLoS One*. 2014;9(2):e88414.

Supplementary materials
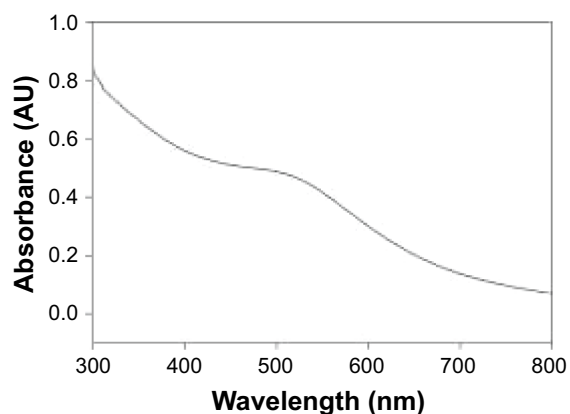
Figure S1 SPB of 3 nm AuNP. UV-Vis spectrum of 3 nm AuNP measured in CHCl₃.
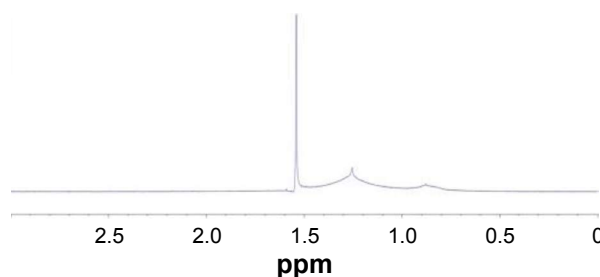**Abbreviations:** AuNPs, gold nanoparticles; SPB, surface plasmon band; UV-Vis, ultraviolet–visible.

Figure S2 ¹H NMR spectra of 3 nm AuNP in CDCl₃.
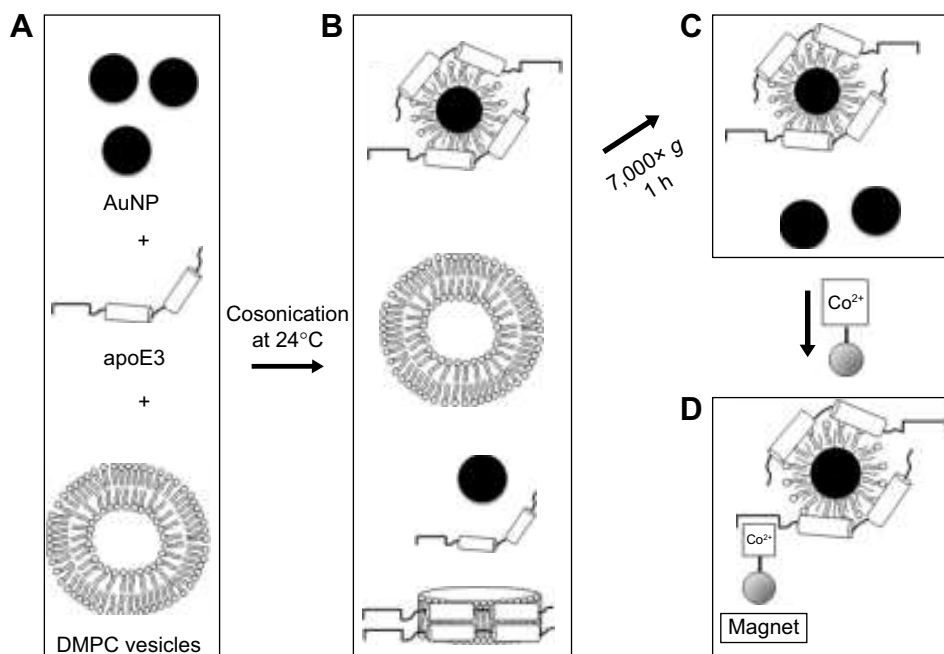**Abbreviations:** AuNPs, gold nanoparticles; NMR, nuclear magnetic resonance.

Figure S3 Purification scheme of rHDL-AuNP. (**A**) Reagents required for synthesis, including AuNP, apoE3, and DMPC vesicles; (**B**) after cosonication and incubation for 16 hours at 24°C, various nanostructures were formed, as well as unreacted reagents; (**C**) centrifugation at 7,000× g for 1 hour removed nanostructures, lipids, and lipid-free apoE3, while rHDL-AuNP and AuNP aggregates remained; (**D**) metal affinity chromatography using Co²⁺-conjugated Dynabeads®, which attracted the His-tag on apoE3 and ensured the removal of AuNP that was not embedded in lipoproteins.
Abbreviations: AuNPs, gold nanoparticles; DMPC, 1,2-dimyristoyl-*sn*-glycero-3-phosphocholine; rHDL, reconstituted high-density lipoprotein.
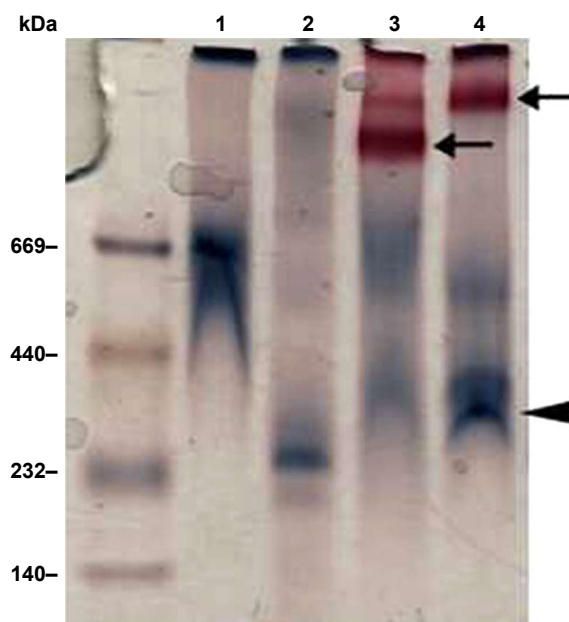
Figure S4 Nondenaturing PAGE of rHDL/rHDL-AuNP. The particles (~50 µg of protein) were electrophoresed on 4%–12% acrylamide gradient gel. The far left lane bears markers with the indicated molecular mass. The lane assignments are as follows: lane 1, rHDL only; lane 2, rHDL-3-nm AuNP; lane 3, rHDL-10-nm AuNP; lane 4, rHDL-17-nm AuNP. Arrows draw attention to rHDL with embedded AuNP; in lane 2, rHDL with 3-nm AuNP appears more diffuse. The arrowhead points to bands that may represent remodeled empty rHDL.
Abbreviations: AuNPs, gold nanoparticles; PAGE, polyacrylamide gel electrophoresis; rHDL, reconstituted high-density lipoprotein.